iScience

Article

Agent-based modeling of neuronal mitochondrial dynamics using intrinsic variables of individual mitochondria

Graphical abstract

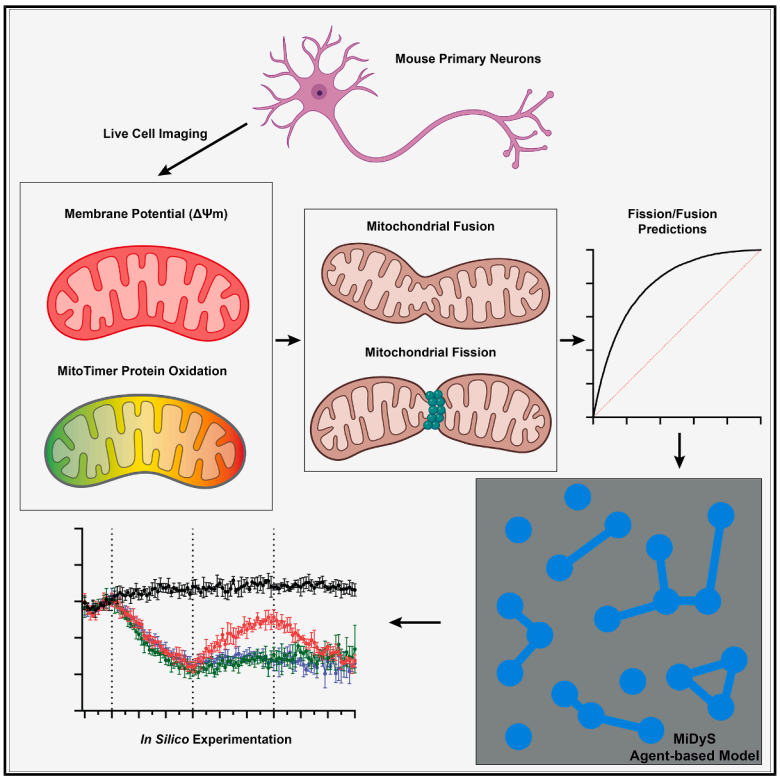

Highlights

- Mitochondrial size and shape influence fission and fusion probabilities
- Physiological mitochondrial membrane potential does not favor fission or fusion
- Mitochondrial fusion occurs more often with higher protein oxidation levels
- Intrinsic mitochondrial properties can be used to model mitochondrial dynamics

Authors

Garrett M. Fogo, Francisco J. Torres Torres, Reagan L. Speas, Anthony R. Anzell, Thomas H. Sanderson

Correspondence

thsand@med.umich.edu

In brief

Molecular biology; Neuroscience; Cell biology

Fogo et al., 2025, iScience *28*, 112390
May 16, 2025
https://doi.org/10.1016/j.isci.2025.112390

CellPress

iScience

CellPress
OPEN ACCESS

Article

Agent-based modeling of neuronal mitochondrial dynamics using intrinsic variables of individual mitochondria

Garrett M. Fogo,[1,2] Francisco J. Torres Torres,[1] Reagan L. Speas,[1] Anthony R. Anzell,[6] and Thomas H. Sanderson[1,3,4,5,7,*]
[1]Neuroscience Graduate Program, University of Michigan, Ann Arbor, MI, USA
[2]Ann Romney Center for Neurologic Diseases, Department Neurology, Brigham and Women's Hospital and Harvard Medical School, Boston, MA, USA
[3]Department Emergency Medicine, University of Michigan, Ann Arbor, MI, USA
[4]The Max Harry Weil Institute for Critical Care Research and Innovation, University of Michigan, Ann Arbor, MI, USA
[5]Department Molecular and Integrative Physiology, University of Michigan, Ann Arbor, MI, USA
[6]Graduate School of Public Health, University of Pittsburgh, Pittsburgh, PA, USA
[7]Lead contact
*Correspondence: thsand@med.umich.edu
https://doi.org/10.1016/j.isci.2025.112390

SUMMARY

Mitochondrial networks undergo remodeling to regulate form and function. The dynamic nature of mitochondria is maintained by the dueling processes of mitochondrial fission and fusion. Dysfunctional mitochondrial dynamics have been linked to debilitating diseases and injuries, suggesting mitochondrial dynamics as a promising therapeutic target. Increasing our understanding of the factors influencing mitochondrial dynamics will help inform therapeutic development. Utilizing live imaging of primary neurons, we analyzed how intrinsic properties of individual mitochondria influence their behavior. We found that size, shape, mitochondrial membrane potential, and protein oxidation predict mitochondrial fission and fusion. We constructed an agent-based model of mitochondrial dynamics, the mitochondrial dynamics simulation (MiDyS). *In silico* experiments of neuronal ischemia/reperfusion injury and antioxidant treatment illustrate the utility of MiDyS for testing hypothesized mechanisms of injury progression and evaluating therapeutic strategies. We present MiDyS as a framework for leveraging *in silico* experimentation to inform and improve the design of therapeutic trials.

INTRODUCTION

Mitochondrial fission and fusion, collectively termed mitochondrial dynamics, remodel the structure of the cellular mitochondrial network.[1–3] Mitochondrial structure is tightly connected to its vital functions.[4,5] Dysfunctional mitochondrial dynamics have been observed in many disease and injury contexts of the brain, including Alzheimer disease, Parkinson disease, stroke, and traumatic brain injury.[6–8] Additionally, perturbed mitochondrial dynamics can aggravate neuronal damage following a primary injury.[9–13] These findings have led to increased interest in therapeutic interventions targeting mitochondria and the molecular machinery that regulate their dynamic behavior.[14]

Computational modeling of biological mechanisms is a growing field, as access to software and resources, along with computer literacy, has significantly increased in recent years. *In silico* experimentation with models of biological systems allows for hypothesis testing and predictive modeling for optimization of experimental design. The predictive power of computational models is particularly valuable for designing preclinical and clinical trials.[15–17] Subject, budgetary, and logistical limitations often complicate the ideal design of therapeutic trials. For example, it is not feasible to test greater than 5–10 possible dosing strategies in a single study while maintaining statistical power and feasibility. Predictive models can be leveraged to identify the therapeutic strategies with the best possible chances of success prior to (pre)clinical trials, therefore minimizing cost, streamlining trial execution, and limiting potential harm.

The complexities of mitochondrial biology have been modeled using mathematical and systems-level techniques.[18–22] Various modeling approaches (e.g., ordinary differential equations, Boolean networks) have been utilized to model mitochondrial dynamics on the order of cells and organisms.[23–27] Because cells and organelles, like mitochondria, are discrete objects with innate abilities to perform certain functions, agent-based modeling is an optimal methodology to create a working model of mitochondrial behavior.[28] Agent-based models are composed of individual agents that have given rule sets to perform actions and interactions. These micro-rule sets can give rise to macro-level patterns of the entire system. Several groups have composed agent-based models of mitochondrial

dynamics yielding insights into the crosstalk of dynamics with motility, mitophagy, and aging.[25,29,30]

The aim of the present study was to identify the relationships between intrinsic variables of individual mitochondria and fission/fusion behavior. To this end, we analyzed the size, shape, mitochondrial membrane potential, and protein oxidation level of mitochondria undergoing fission and fusion in mouse primary neurons. We synthesized our findings into an agent-based model of mitochondrial dynamics, called the mitochondrial dynamics simulation (MiDyS). Further, we illustrate the potential utility of MiDyS for *in silico* experimentation with simulated ischemia/reperfusion (I/R) injury and therapeutic intervention.

RESULTS

Dynamic mitochondria have distinct intrinsic properties

To investigate the relationships between intrinsic properties of individual mitochondria and their behavior, we utilized live cell microscopy with fluorescent mitochondrial labeling. The size and shape of individual mitochondria is the result of mitochondrial fission and fusion. The size, shape, and proximity of mitochondria also directly influence the processes of mitochondrial dynamics. Mitochondrial membrane potential ($\Delta\Psi$) is the electrochemical gradient formed across the mitochondrial inner membrane that is critical for oxidative phosphorylation and has been shown to influence the balance of mitochondrial dynamics.[31,32] Therefore, we labeled mitochondria in mouse primary cortical neurons with 30 nM MitoTracker Deep Red (MTDR). MTDR is a fluorescent dye whose uptake to the mitochondrial matrix is dependent on the mitochondrial membrane potential, allowing analysis of mitochondrial morphology and mitochondrial membrane potential.[33,34] Mitochondrial networks were imaged every 60 s over a period of 30 min to capture dynamic changes and the corresponding relative mitochondrial membrane potential (Figure 1A). Image sequences were then analyzed for identification of mitochondrial fission and fusion events using ROI-based automated detection script in FIJI.[35] If a mitochondrial object was detected to perform fission or fusion between frame^{n-1} and frame^{n}, the mitochondrial object would be tagged, and measurements would be taken from frame^{n-1} (Figure 1B). Area distribution was analyzed to reflect mitochondrial size, aspect ratio for mitochondrial shape, and MTDR signal for relative mitochondrial membrane potential of each mitochondrial object undergoing fission, fusion, and objects that remained unchanged. A total of 105,958 mitochondrial objects were analyzed, with 29,627 and 15,386 objects undergoing fusion and fission, respectively. MTDR mean intensity within mitochondrial objects remained stable throughout the recording periods (Figure 1C). We observed a balance between fusion (18.18%) and fission (16.62%) events (quantified as percentage of total mitochondria), with slight favor to fusion during MTDR recordings (Figure 1D).

Mitochondrial fission and fusion have been proposed to organize mitochondrial proteostasis, mitochondrial DNA nucleoids, and ultrastructure.[36–38] We sought to determine if mitochondrial protein status altered dynamics. To this end, we crossed Thy1-Cre[39] mice with conditional MitoTimer mice for neuron-specific expression of MitoTimer protein.[40,41] MitoTimer is a designer protein that fluoresces green when newly synthesized and trafficked to the mitochondrial matrix. Oxidation of MitoTimer, whether over time or due to oxidative stress, causes an irreversible shift in fluorescence to red. The MitoTimer red/green ratio therefore is an indicator of the balance between new and old/oxidized protein within the mitochondria.[40,41] Live cell recordings were taken of MitoTimer-expressing primary neurons over 30 min. MitoTimer neurons were imaged every 120 s over this period to limit photobleaching. MitoTimer recordings were then analyzed for fission and fusion events (Figures 1E and 1F). Similar to MTDR recordings, mitochondrial fluorescence remained stable over time with a balance of fusion (14.26%) and fission (11.49%) events (Figures 1G and 1H). A total of 20,437 MitoTimer-expressing mitochondria were analyzed with 1,963 fission- and 3,208 fusion-tagged objects.

The distribution of intrinsic variables was assessed across three groups of labeled mitochondria: stable, fission, and fusion. Mitochondrial area was found to be differentially distributed among the three groups. Fission objects had a shift toward larger mitochondrial area (6.924 ± 12.82 μm^2), whereas the fusion group (1.772 ± 3.099 μm^2) demonstrated a wider variability of area compared to stable mitochondria (2.575 ± 6.304 μm) (Figure 2A). This finding appears logical as parent mitochondria must be large enough to produce two viable daughter mitochondria when undergoing fission, whereas fusion can be performed by even the smallest viable mitochondrial object. Aspect ratio (AR), the ratio between the longest (major) and shortest (minor) axis of an object's fitted ellipse, was similar between stable (2.881 ± 1.916) and fusion objects (2.836 ± 1.862). However, fission objects had a shifted AR distribution (4.219 ± 2.614), indicating a higher likelihood of long linear objects in that group (Figure 2B). MTDR signal was quantified as the mean intensity of MTDR within each mitochondrial object relative to the mean intensity of the entire image. Mitochondria from all three groups had similar central values of MTDR intensity; however, fission or fusion objects were more likely to have MTDR values near the outer limits of the distribution (Figure 2C). These data suggest mitochondrial membrane polarization outside of the baseline range is associated with dynamic behavior. In MTDR recordings, MTDR relative intensity did not have strong correlations with any size or shape descriptors (Figure 2D). The distribution of MitoTimer ratio in analyzed mitochondria was a nonnormal distribution in all three groups. Distributions for stable (0.2620 ± 0.1050) and fission objects (0.2829 ± 0.1047) appeared to follow a sum of two Gaussian distributions. Fusion mitochondria were more distributed on the higher end of MitoTimer ratio (0.3341 ± 0.1165), suggesting that fusion is associated with older or more oxidized proteins (Figure 2E). Similar to MTDR, MitoTimer ratio did not correlate strongly with other variables (Figure 2F). Our results from primary neuron recordings identify distinct features of mitochondria prior to fission and fusion, wherein fission mitochondria are more likely to be larger linear objects and fusion mitochondria are more likely to have altered protein oxidation levels. Additionally, fusion or fission mitochondria are more likely than stable mitochondria to have membrane potentials that deviate from a normal range.

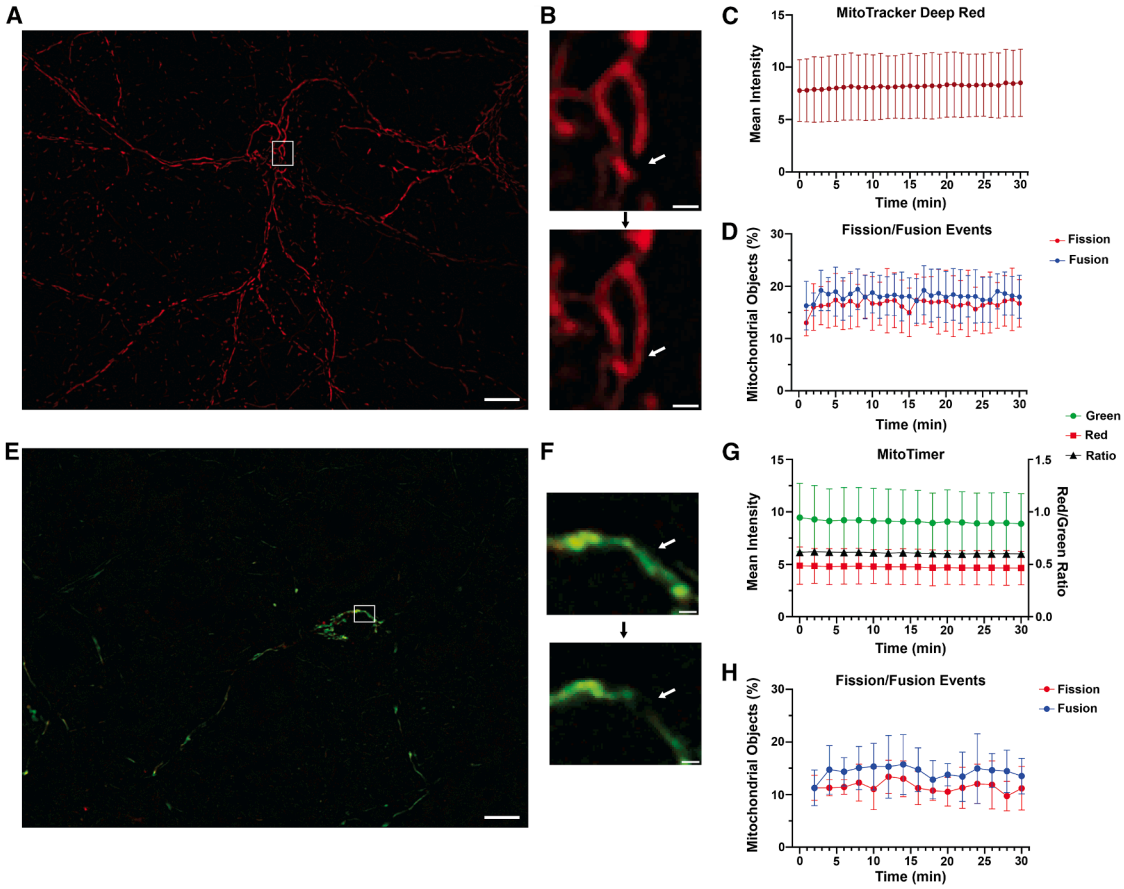

Figure 1. Neuronal recordings of mitochondrial dynamics

(A) Representative image of MitoTracker Deep Red-labeled neurons from live cell recordings. Scale bar: 10 μm.

(B) Representative frames 60 s apart of MitoTracker Deep Red-labeled mitochondria performing fusion. Scale bar: 1 μm.

(C) Quantification of MitoTracker Deep Red signal over time in neuron recordings.

(D) Quantification of mitochondria undergoing fusion and fission events, as percentage of total mitochondrial objects, over time in MitoTracker Deep Red recordings.

(E) Representative image of MitoTimer neuron from live cell recordings. Scale bar: 10 μm.

(F) Representative frames 120 s apart of MitoTimer expression mitochondria performing fission. Scale bar: 1 μm.

(G) Quantification of MitoTimer green signal, red signal (left y axis), and red/green ratio (right y axis) over time in MitoTimer neuron recordings.

(H) Quantification of mitochondria undergoing fusion and fission events, as percentage of total mitochondrial objects, over time in MitoTimer recordings. n = 4–5 biological replicates.

Prediction of mitochondrial fission/fusion events

Due to the distinct properties of fusion and fission mitochondria, we evaluated our ability to predict mitochondrial behavior using measured intrinsic values. During our recordings, we identified many mitochondrial objects that could perform fusion and fission within the 60–120 s intervals; therefore, we decided to split our predictions into stable vs. fusion and stable vs. fission, rather than a three-way decision. The overlapping fluorescent spectra between the red MitoTimer and MTDR did not allow us to record data of both reporters from the same mitochondria. This led us to generate two separate prediction models for each reporter. Multiple logistic regression was performed on stable, fission, and fusion mitochondria, with mitochondrial area, major, minor, AR, and MTDR or MitoTimer as the inputs with stable being the negative outcome and fission or fusion being the positive outcome. Prediction fission from MTDR and MitoTimer data produced ROC curves with area under the curve (AUC) of 0.7926 and 0.8485, respectively (Figures 3A and 3E). Both regressions produced similar predicted probability distributions with high negative predictive power (Figures 3B and 3F). Fusion regressions had lower AUC values (0.6497 and 0.7370) and less negative predictive power (Figures 3C, 3D, 3G, and 3H). Fusion prediction was predicted to be more difficult as the behavior of two or more mitochondria must be predicted, compared to fission that requires only one parent mitochondria.

Agent-based model of mitochondrial dynamics

Agent-based models utilize rule sets given to individual autonomous agents, wherein the actions and interactions of the agents produce the dynamics of the overall simulated network/environment. We applied our data from individual

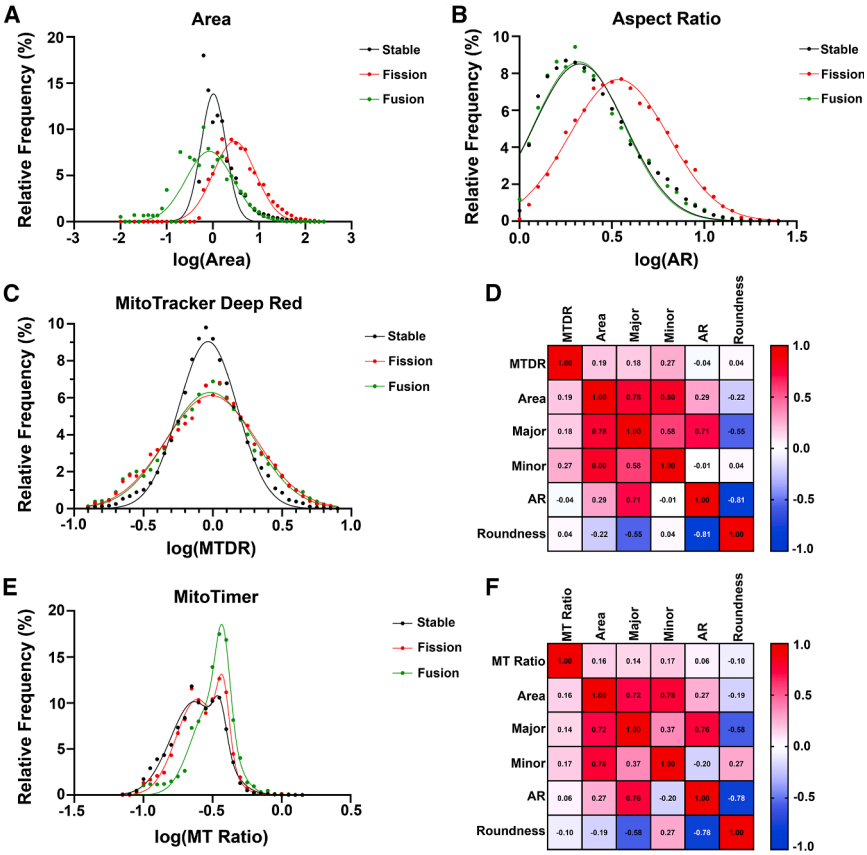

Figure 2. Dynamic mitochondria have unique intrinsic properties

(A) Histogram of log-transformed mitochondrial area (μm^2) from individual mitochondrial objects during MTDR recordings. Curves are fitted Gaussian distributions.

(B) Histogram of log-transformed aspect ratio (AR) from individual mitochondrial objects during MTDR recordings. Curves are fitted Gaussian distributions.

(C) Histogram of log-transformed relative MitoTracker Deep Red (MTDR) mean intensity from individual mitochondrial objects during MTDR recordings. Curves are fitted Gaussian distributions.

(D) Correlation matrix of intrinsic variables collected from individual mitochondrial objects during MTDR recordings.

(E) Histogram of log-transformed MitoTimer red/green ratio from individual mitochondrial objects during MitoTimer recordings. Curves are sum of two Gaussian distributions.

(F) Correlation matrix of intrinsic variables collected from individual mitochondrial objects during MitoTimer recordings.

mitochondria and logistic regressions to construct an agent-based model of mitochondrial dynamics in NetLogo, an open-source agent-based modeling program.[42] Our model, called MiDyS, is composed of a single-cell simulation environment with agents representing the smallest measured mitochondrial objects. Agents (circles) in the simulation can move and perform interactions with other agents to model dynamic behavior. Agents create and destroy fusion links with other agents to simulate mitochondrial fusion. Alternatively, fission is modeled by the loss of a link between two agents to form two smaller objects. The number of agents in the simulation is controlled by simulated biogenesis (growth of new linked agent from parent agent) and mitophagy (loss of unlinked agent). Each agent can perform any of these four functions, each interval simulating 1 min of time progression (Figure 4A). The MiDyS simulation environment represents a single cell (2500 μm^2) made up of 50 $\times$ 50 patches of 1 $\times$ 1 μm^2 (Figure 4B). Mitochondrial agents are each 0.5 μm^2 in size and have encoded intrinsic properties, including membrane potential and MitoTimer ratio. When an agent creates a fusion link with another agent, those agents represent a continuous mitochondrial agent; therefore, size and shape parameters are measured by mitochondrial object. Conversely, membrane potential and MitoTimer ratio are not equilibrated across mitochondrial objects and are rather localized to the individual agents within an object. This mirrors the spatial restriction of membrane potential and protein homeostasis observed in cells.[43–45] The NetLogo interface of MiDyS allows for precise control of starting parameters including number of agents and initial networking density on the left side of the interface. The simulation window is located in the center of the interface for visualization of mitochondrial dynamics. Custom output plots and monitors on the interface allow real-time and exportable data analysis of global and agent-specific parameters (Figure 4B).

The fission and fusion actions of agents are determined by the multiple logistic regression equations derived from *in vitro* neuron data. Intrinsic values of mitochondrial agents are input to the regression model and the result represents the probability of fission/fusion. After calculation, each agent runs probability checks for fission and fusion, giving rise to the stochastic agent-based dynamics of MiDyS. Because two regression models were generated for both fusion and fission, agents perform both calculations and keep the larger value. The processes of mitochondrial biogenesis and mitophagy were not directly evaluated in our *in vitro* recordings, and therefore, we used assumed rates based on literature review and other models.[25,30,46] Biogenesis occurs at a rate of 5% for agents that fall within the baseline range of membrane potential, due to import of new protein in mitochondria being dependent on mitochondrial membrane potential.[47,48] Mitophagy occurs at a rate of 10% for agents that have no links; this assumption is based on previous data from our group showing that mitophagy in primary neurons heavily favors mitochondrial objects < 1 μm^2 in area.[46,49] Simulations over time in MiDyS present stable balances of fusion and fission events over time with visualization of individual dynamics events and micro-interactions between agents (Figure 5).

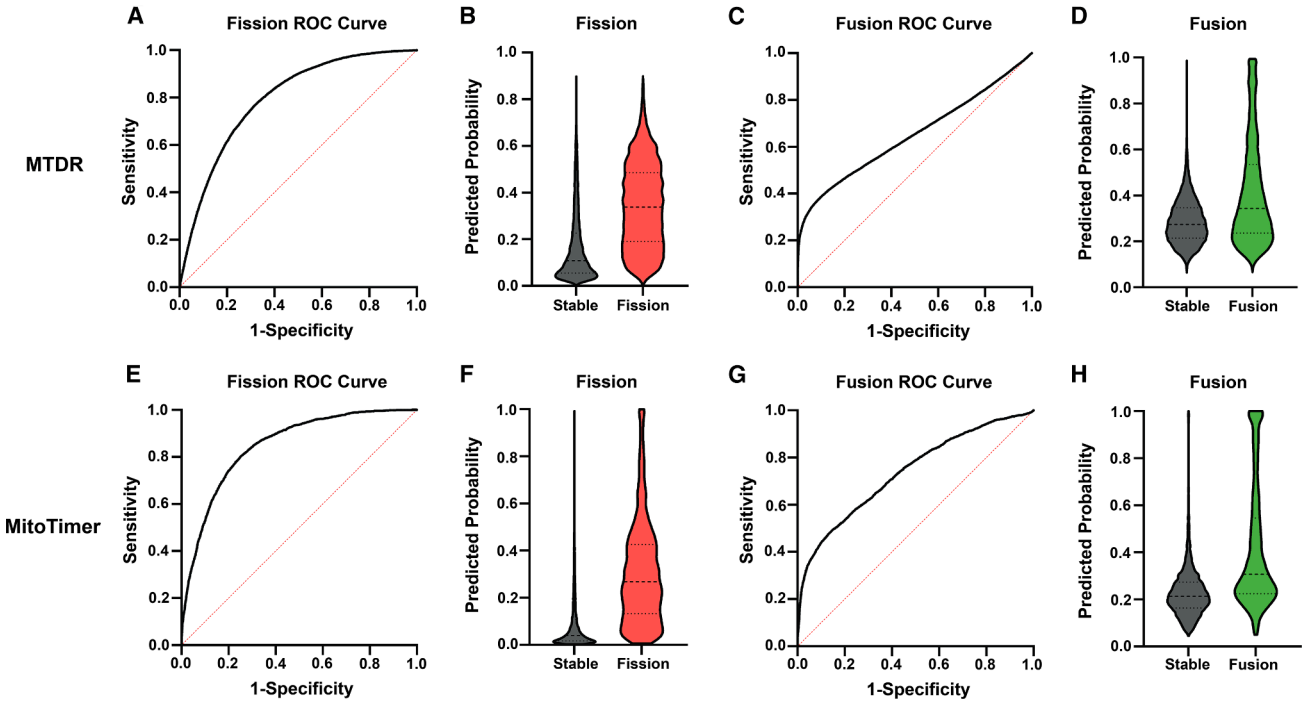

Figure 3. Intrinsic mitochondrial properties predict fission and fusion events

(A) ROC curve of multiple logistic regression classifying stable and fission mitochondria from MTDR recordings.
(B) Violin plot of predicted probability for fission of MTDR-labeled mitochondria by multiple logistic regression.
(C) ROC curve of multiple logistic regression classifying stable and fusion mitochondria from MTDR recordings.
(D) Violin plot of predicted probability for fusion of MTDR-labeled mitochondria by multiple logistic regression.
(E) ROC curve of multiple logistic regression classifying stable and fission mitochondria from MitoTimer recordings.
(F) Violin plot of predicted probability for fission of MitoTimer mitochondria by multiple logistic regression.
(G) ROC curve of multiple logistic regression classifying stable and fusion mitochondria from MitoTimer recordings.
(H) Violin plot of predicted probability for fusion of MitoTimer mitochondria by multiple logistic regression.

Simulated ischemia/reperfusion injury alters mitochondrial dynamics

One of the goals for MiDyS was to demonstrate the utility of agent-based modeling for *in silico* experimentation. MiDyS was therefore encoded with the ability to manipulate key intrinsic variables of the agents. Sliders on the interface allow users to manipulate the membrane potential and MitoTimer ratio by defined increments over time. This allows users to simulate disease/injury models of interest associated with oxidative stress and/or depolarization/hyperpolarization. Cerebral I/R injury is a leading cause of death and disability, as well as a known effector of oxidative stress, mitochondrial membrane potential, and mitochondrial dynamics.[7,50–52] We therefore set out to simulate neuronal I/R injury in MiDyS. There are several leading models of mitochondrial membrane potential and oxidative stress temporal dynamics considered in I/R. We tested the outcomes of three models differing in the timing of mitochondrial membrane potential and reactive oxygen species (ROS) production: ischemia-induced ROS,[53–55] hyperpolarization-induced ROS,[52,56,57] and reperfusion-induced ROS[58,59] (Figure 6). We found that simulated ischemia in all three models produced extensive mitochondrial fragmentation and reduced fusion probability. Mitochondrial fission was inhibited in all models upon reperfusion, but fusion increased only in the hyperpolarization-induced ROS model. Late-stage reperfusion then induced a secondary phase of mitochondrial fission in the hyperpolarization-induced ROS model. This temporal pattern of ischemia-induced fission, early fusion during reperfusion, and secondary fragmentation matches previous observations of neuronal mitochondrial dynamics following I/R[46,60,61] (Figure 6). The changes in mitochondrial membrane potential of the hyperpolarization-induced ROS model were reduced to keep values within physiological range, and the pattern of fusion and fission remained consistent (Figures 7A–7F). The balance of mitochondrial fission and fusion in MiDyS is quantified by the fission/fusion index (FFI), ranging from −1 (complete fission) to 1 (high fusion) (Figure 7F). The pattern of mitochondrial fission and fusion observed in the MiDyS-simulated ischemia model mirrored patterns of dynamics observed in primary neuron oxygen-glucose deprivation and reoxygenation (OGD/R), an *in vitro* model of I/R injury (Figures 7G and 7H).

In silico experimentation defines therapeutic window of antioxidants

With the establishment of a simulated I/R paradigm, we proceed to test a simulated preclinical trial. Historically, antioxidants have been leading candidates for therapeutic intervention during

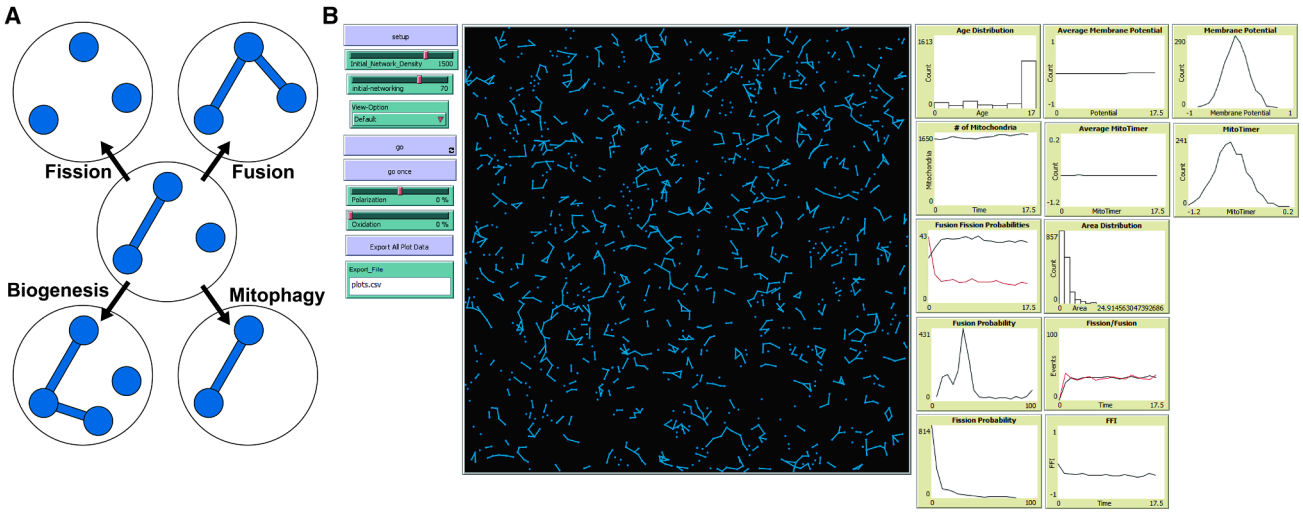

Figure 4. MiDyS: an agent-based model of mitochondrial dynamics

(A) Agents in MiDyS are circles that represent the smallest functional mitochondrial object. Fusion links can be made between agents to create larger mitochondrial objects. Agents can perform four actions with each tick (1 min): fission (loss of link to other agent), fusion (creation of new link to other agent), biogenesis (growth of new connected agent), and mitophagy (loss of unlinked agent).

(B) MiDyS model interface in NetLogo. Start/stop buttons, starting parameters, and export parameters are listed to the left of the central visualization panel. Mitochondrial dynamics can be visualized in the center window. To the right are live output plots of key network diagnostics and individual mitochondrial variables, including area, membrane potential, and fusion/fission probabilities.

cerebral I/R injury.[62–65] Because the extent of oxidative stress applied to agents can be simply adjusted in our model, we chose to simulate antioxidant therapy during I/R injury. A critical issue in designing preclinical and clinical trials is the determination of discrete treatment groups. Dose, delivery strategy, and timing are all key variables that must be considered. Selection of inopportune variables can contribute to negative and/or misleading results. Predictive modeling and *in silico* experimentation with MiDyS and similar programs can aid these critical decisions by quantitatively comparing outcomes with different combinations of variables. To demonstrate this, we set out to determine the therapeutic window for antioxidant therapy in our simulated I/R model. Treatment of acute brain injuries require defined therapeutic windows, as minutes can separate distinct pathological mechanisms and render a therapy beneficial, inert, or even detrimental.[66–69] We simulated application of antioxidant therapy (reduction of oxidative stress by 40%) at the onset of reperfusion to first demonstrate therapeutic efficacy. Antioxidant therapy preserved mitochondrial content and mitochondrial morphology through the inhibition of mitochondrial fission probability (Figure 8A). Next, we delayed antioxidant treatment by 5, 10, 20, and 25 min to determine the therapeutic window. Delayed treatments had incremental changes in total oxidation and provided diminishing returns of therapeutic effect on mitochondrial content and morphology (Figures 8B and 8C). Simulated data suggest that antioxidant therapy loses rescue of mitochondrial content at 20 min of delay and rescue of mitochondrial morphology at 25 min of delay. Utilizing these observations, one could make an informed decision about the cutoff time for enrollment of patients in a clinical trial of antioxidant therapy for cerebral I/R injury. These *in silico* experiments demonstrate the potential utility of MiDyS and similar predictive models for experimental and trial design.

DISCUSSION

Mitochondrial dynamics are implicated in numerous disease and injury models of the brain. The field requires an intimate knowledge of the key factors contributing to mitochondrial fission and fusion in order to target and treat these pathologies. As individual mitochondria are discrete organelles with their own genomes and proteomes, we set out to define the relationships between the intrinsic properties of individual mitochondria and their respective dynamic behavior. We found that larger linear mitochondria are more likely to undergo fission, and mitochondria with older/more oxidized proteins are more likely to perform fusion. Additionally, deviation from the basal range of mitochondrial membrane potential is associated with dynamic events, including both fusion and fission. Leveraging our collected datasets, we generated an agent-based model of neuronal mitochondrial dynamics, termed MiDyS. Simulations in MiDyS present balanced mitochondrial networks capable of replicating temporal patterns of mitochondrial dynamics in neuronal I/R injury. Further, we illustrated the potential application of MiDyS for simulated (pre)clinical trials by testing the effects of delayed antioxidant therapy after I/R. We believe that MiDyS can be a framework for the study of mitochondrial dynamics *in silico* and development of future therapeutic strategies targeting mitochondria.

Our live cell imaging results suggest that objects undergoing mitochondrial fission tend to be larger and more linear than stable and fusing mitochondria. Logic tells us that fission into two daughter mitochondria would require a parent mitochondrial object at least double the minimum size of a mitochondrial object, which aligns with our data. Kleele et al.[70] describe a model for distinct mechanisms of mitochondrial fission based on scission location. Although not the primary target of the study, their

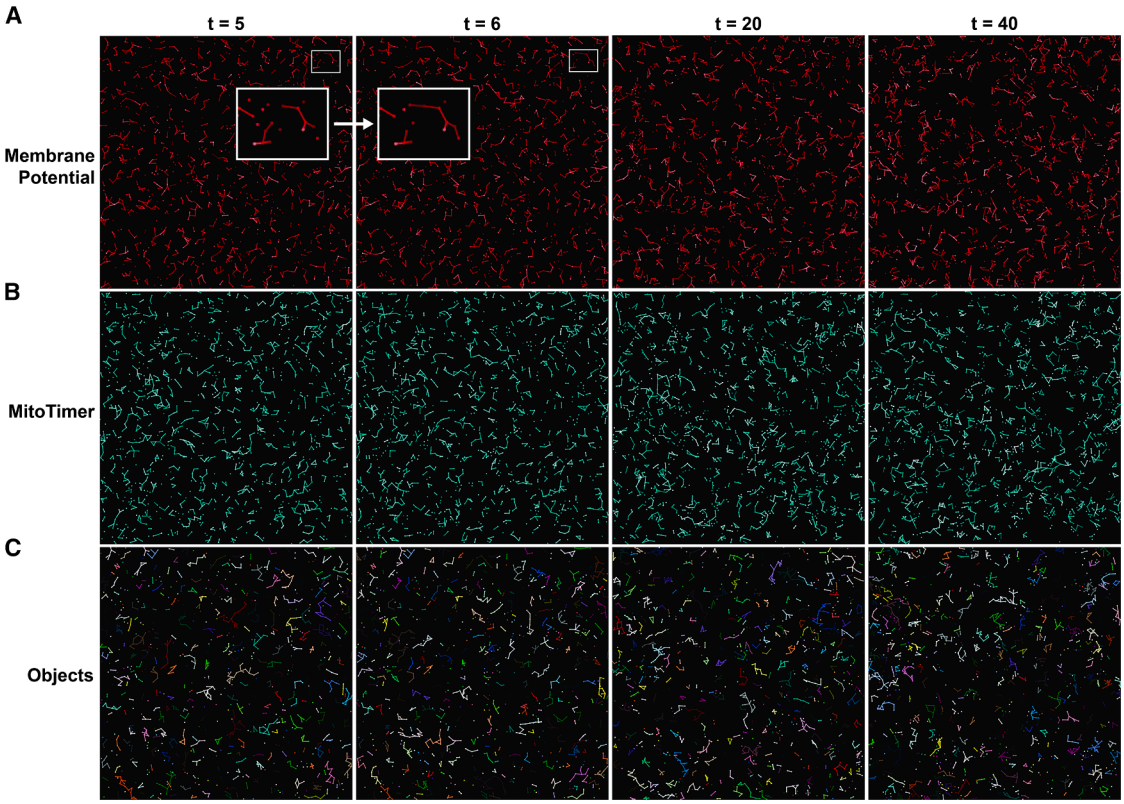

Figure 5. MiDyS allows for modeling and visualization of fission/fusion dynamics

(A) Representative images of MiDyS membrane potential visualization over simulated time. Insert: zoomed frames demonstrating fusion and fission.

(B) Representative images of MiDyS MitoTimer visualization over simulated time.

(C) Representative images of color-coded mitochondrial objects in MiDyS over time.

data also demonstrate that larger daughter mitochondrial objects after fission are more likely to undergo fission than fusion. MitoTimer ratio was not found to be different in fission mitochondria compared to stable mitochondria, although both populations demonstrated two peak populations of MitoTimer ratio, rather than a normal distribution. These two populations may be separated by location of the scission point, as Kleele et al.[70] additionally demonstrated that high mitochondrial ROS levels are associated with peripheral fission (fission near the end of the mitochondrial object) and not midzone fission. The lack of association between MitoTimer ratio and fission was surprising, as oxidative stress is a well-demonstrated inducer of mitochondrial fission in many contexts.[71–73] However, it is important to note that MitoTimer is not a specific or exclusive reporter of mitochondrial ROS levels.[40,41] Krzystek et al.[74] additionally found that a highly red (oxidized) MitoTimer ratio is not an exclusive determinant of fission or mitophagy. Considering MitoTimer as an indicator of protein age also suggests that mitochondrial fission is not influenced by protein dynamics. Mitochondria in dividing cells use fission to sort mitochondria by protein age[75]; however, we did not analyze MitoTimer ratio in daughter mitochondria and therefore cannot conclude if this is also true in post-mitotic neurons.

Mitochondria on the outer bounds of the mitochondrial membrane potential spectrum displayed more incidence of dynamic behavior. Interestingly, the distribution of mitochondrial membrane potential was similar between fission and fusion objects. Treatment of cells with toxins causing mitochondrial depolarization (e.g., FCCP) and hyperpolarization (e.g., oligomycin) generally produce mitochondrial fragmentation.[76–78] Because our recordings only included neurons at control conditions, it is likely that we only captured physiological levels of mitochondrial membrane potential. Our data suggest that in this range, fusion and fission are just as likely to occur, whereas treatment with mitochondrial toxins may push mitochondrial membrane potential to super physiological levels. Our data are contrasted by a previous study that demonstrated depolarized daughter mitochondria after fission are less likely to fuse than the more polarized daughter.[79] It is unclear if this effect is only true in the acute phase after fission or universal. Fusion mitochondria were more likely to have higher MitoTimer ratios, indicating a greater abundance of oxidized protein compared to new protein. These data compliment the findings from Ferree et al.,[80] wherein mitochondrial fusion is required to equilibrate MitoTimer signal across the mitochondrial network. Collectively, these findings suggest that mitochondria may have an ability to sense protein homeostasis and use it to trigger fusion for proteostatic equilibration across the entire mitochondrial network.

We culminated our live cell imaging data into a computational model of mitochondrial dynamics (MiDyS). Due to the individual

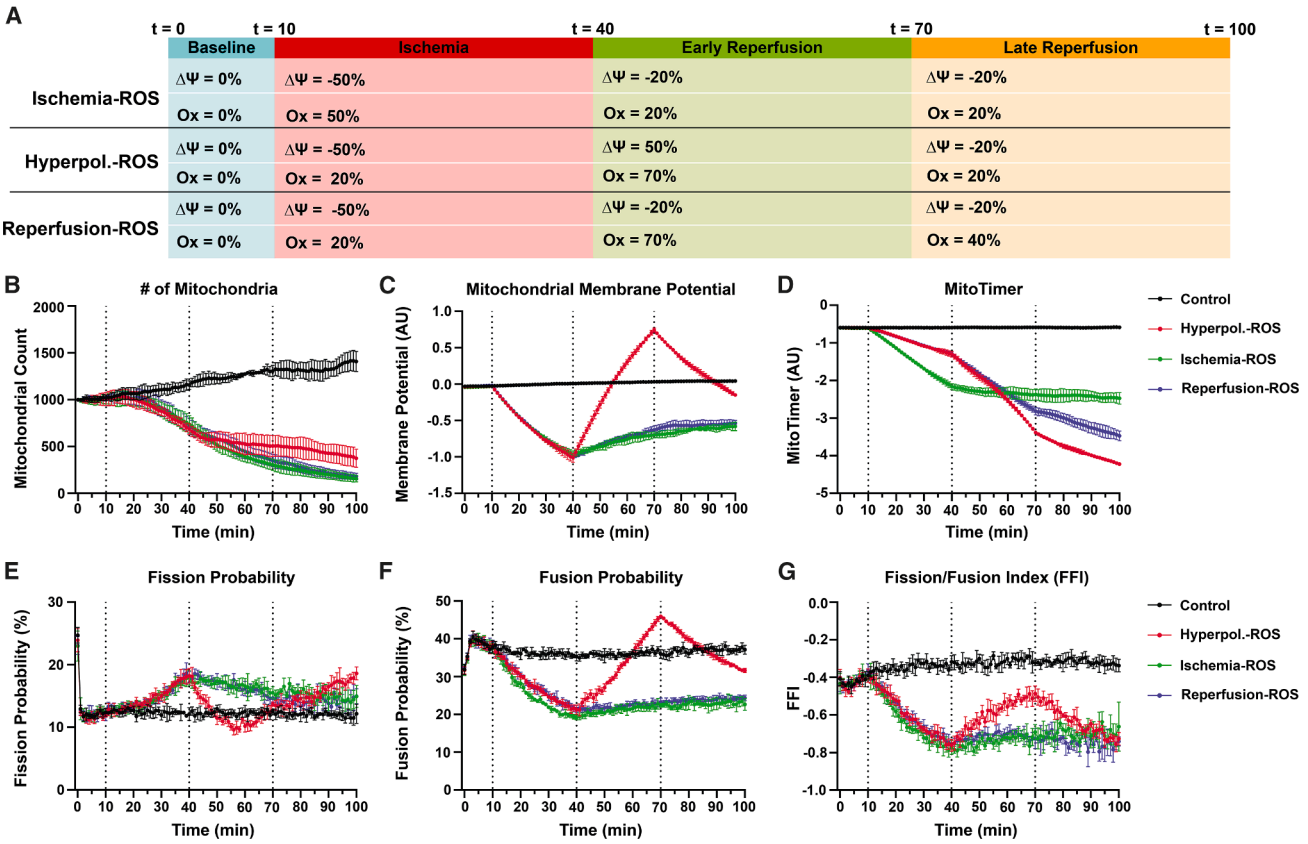

Figure 6. Simulated models of ischemia/reperfusion injury

(A) Timeline and table presenting the manipulations to mitochondrial membrane potential (ΔΨ) and oxidative stress (Ox) during the given phases of simulated I/R.

(B) Quantification of mitochondrial count during I/R simulations.

(C) Quantification of mean mitochondrial membrane potential during I/R simulations.

(D) Quantification of mean MitoTimer during I/R simulations.

(E) Quantification of mean fission probability during I/R simulations.

(F) Quantification of mean fusion probability during I/R simulations.

(G) Quantification of fission/fusion index (FFI) during I/R simulations. Dashed lines separate phases of I/R injury.

nature of mitochondria, we chose to use an agent-based modeling approach, in which individual mitochondrial agents can perform fusion and fission by defined rule sets. Multiple logistic regressions leveraging intrinsic variables of individual mitochondria from our neuronal recordings composed the basis of our stochastic model. In MiDyS, individually encoded parameters of size, shape, membrane potential, and MitoTimer ratio determine the actions and interactions of agents, which give rise to patterns of mitochondrial dynamics comparable to *in vitro* observations. Other groups have similarly leveraged agent-based modeling for the study of mitochondrial dynamics.[29,30] While other models have focused on hypothesis testing of fundamental mitochondrial questions, the aim of MiDyS was to produce a framework for informing future investigations. We based the stochastic equations of our model on *in vitro* observations of variables of interest. The parameters of those *in vitro* experiments define the usefulness but also limitation of our model. MiDyS currently represents a model of how mitochondrial size, shape, membrane potential, and protein homeostasis affects fusion and fission dynamics in cultured neurons. Results and conclusions made beyond this context should therefore be taken with caution. We believe that MiDyS is a framework that can be further developed and improved for many more applications and contexts. A multitude of known and unknown biological factors likely influence mitochondrial dynamics beyond the variables in this study, including Ca^{2+}, ATP, kinase activity, temperature, and pH. Integration of MiDyS with data describing these factors, as well as other models of mitochondrial biology has the potential to greatly enhance its utility and improve future investigations.

We applied MiDyS to simulate proposed models of mitochondrial membrane potential and oxidative stress during I/R injury. The three models consider differing peaks of ROS production and amplitudes of membrane polarization. We then evaluate each mechanism by comparing MiDyS results to known patterns of neuronal I/R mitochondrial dynamics. The first model (Ischemia-ROS) considers the ischemic phase of the injury to be the major producer of ROS, with limited ROS production and effects on mitochondrial membrane potential during reperfusion.[53–55,82] The second model (hyperpolarization-ROS)

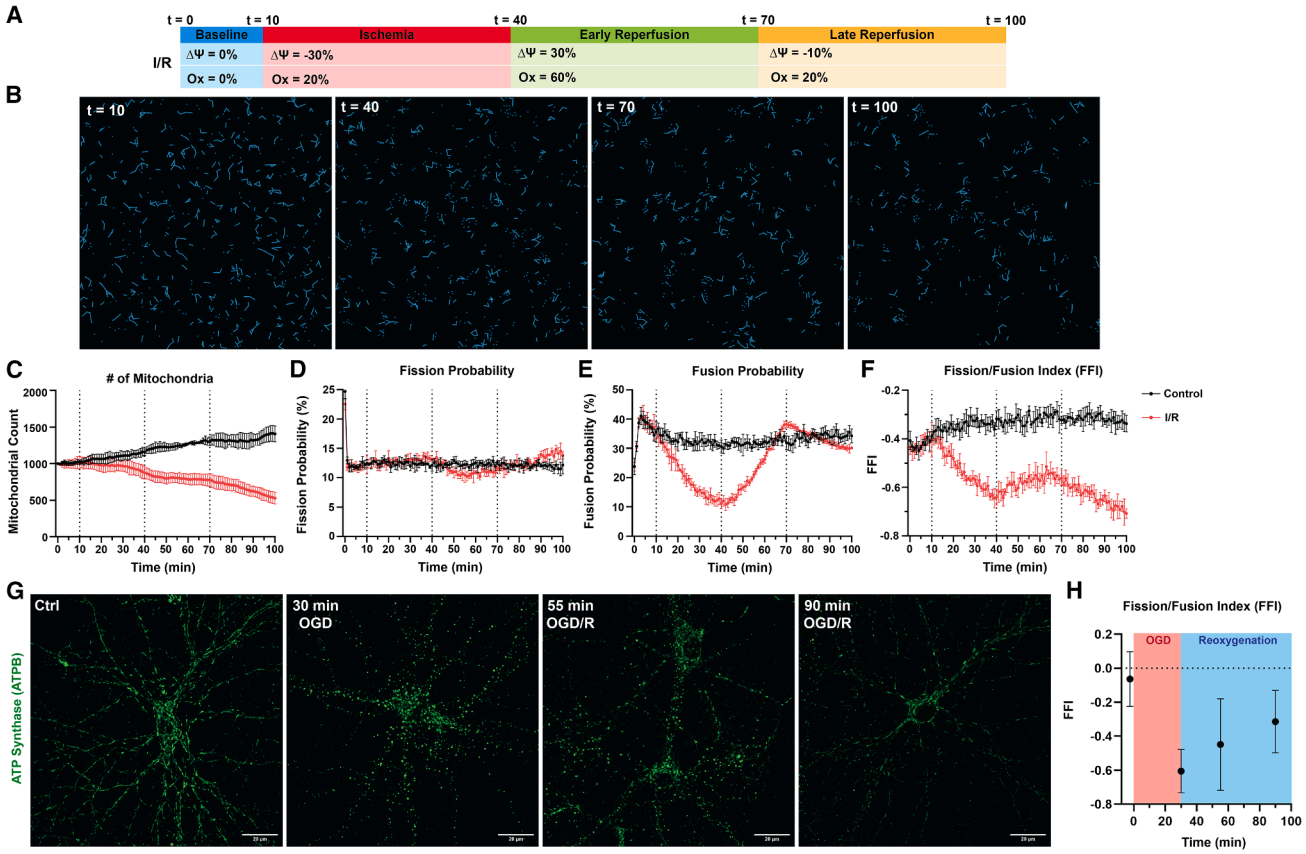

Figure 7. Simulated ischemia/reperfusion injury alters mitochondrial dynamics

(A) Timeline of simulated ischemia/reperfusion (I/R) injury paradigm in MiDyS with manipulation parameters.

(B) Representative images of MiDyS at the conclusion of each phase of I/R simulation.

(C) Quantification of mitochondrial count during I/R simulation.

(D) Quantification of mean fission probability during I/R simulation.

(E) Quantification of mean fusion probability during I/R simulation.

(F) Quantification of fission/fusion index (FFI) during I/R simulation. Dashed lines separate phases of I/R injury.

(G) Representative images of mouse primary neuronal mitochondria (green, ATPB) in control (Ctrl) condition, after 30 min of OGD, OGD + 25 min of reoxygenation (55 min), and OGD + 60 min reoxygenation (90 min).

(H) Quantification of fission/fusion index (FFI) in mouse primary cortical neurons throughout the OGD/R paradigm. n = 4–10 biological replicates, 2–3 separate experiments.

postulates that hyperpolarization of the mitochondrial membrane potential drives ROS production during the early stages of reperfusion, with the limited presence of ROS during ischemia.[52,56,57] The third model (reperfusion-ROS) follows a similar ROS pattern to hyperpolarization-ROS with ROS peaking during reperfusion, but in this model ROS production is not dependent on hyperpolarization.[58,59,83,84] Interestingly, only the hyperpolarization-ROS model generated a fission/fusion pattern similar to *in vitro* and *in vivo* models of neuronal/brain I/R injury.[46,60,61,85] These results highlight hyperpolarization and ROS during early reperfusion may be required for the slowing of mitochondrial fission and mild rebuilding of the mitochondrial network.

Collectively, our results identify unique characteristics of mitochondria prior to fission and fusion. We can leverage these distinct intrinsic properties to predict fission and fusion events. Using an agent-based modeling approach, we constructed a predictive computational model of mitochondrial dynamics. We believe this model can serve as a foundational tool for the study of mitochondrial dynamics and be utilized to inform and improve therapeutic trials targeting mitochondria.

Limitations of the study

Conclusions from the data collected in this study and produced by MiDyS should not be extended outside of its original context. Live cell imaging was performed in mouse primary cortical neurons, a post-mitotic cell type with distinct cellular compartments (e.g., axon, dendrites). It is therefore unlikely that all observations of mitochondrial behavior directly translate to other cell types of interest. Analysis of mitochondria within neurons was equalized across all cellular compartments. A limitation of the fusion and fission event identification algorithm utilized in this study is that mitochondrial motility is not taken into account. It is therefore possible that highly mobile mitochondria could arise as false

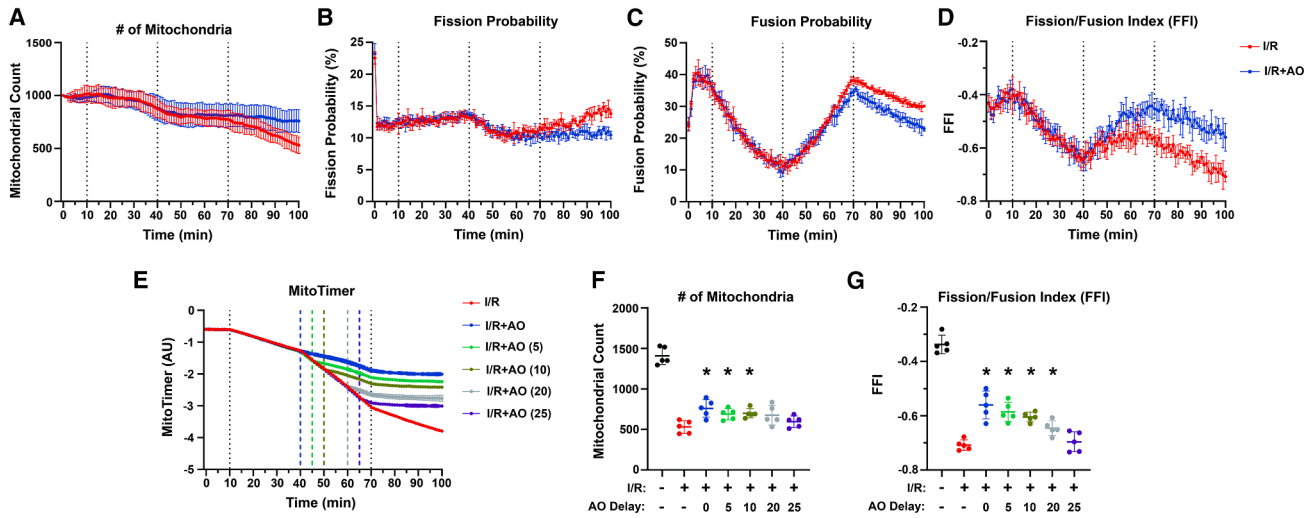

Figure 8. *In silico* experimentation predicts therapeutic window for antioxidant therapy

(A) Quantification of mitochondrial count during I/R simulation with antioxidant (AO) treatment at onset of reperfusion.

(B) Quantification of mean fission probability during I/R + AO simulation.

(C) Quantification of mean fusion probability during I/R + AO simulation.

(D) Quantification of fission/fusion index (FFI) during I/R + AO simulation.

(E) Quantification of mean MitoTimer during I/R with delayed AO treatment simulations. Minutes of delay is shown in parentheses for AO treatment.

(F) Quantification of mitochondrial count at conclusion of I/R simulation with delayed AO treatment. * indicates $p < 0.05$ compared to I/R condition.

(G) Quantification of fission/fusion index (FFI) at conclusion of I/R simulation with delayed AO treatment. * indicates $p < 0.05$ compared to I/R condition.

positives or negatives. We believe this issue is minimal due to the speed of mitochondrial transport observed in our recordings but should still be considered as a limitation. MiDyS is a computational model meant to inform future experiments and is limited by the variables encoded and assumptions made during development. Dynamics of mitochondrial biogenesis and mitophagy were not based on *in vitro* data collected in this study. Future work will be required to optimize stochastic equations for these behaviors. A critical limitation of agent-based modeling is the underestimation of global or environment-driven parameters on agent behavior. For example, mitochondrial fission is known to be influenced by mitochondria-ER contact sites.[81] Unless encoded by another species of agents, the influence of ER tubules on mitochondrial dynamics is not represented.

The data described in this study should also be interpreted based upon the measures used for mitochondrial parameters. The MitoTimer reporter provides a readout of protein oxidation, a variable seemingly interconnected with ROS accumulation. However, MitoTimer is an imperfect reporter for ROS, as transient waves of ROS production will not be captured. Additionally, mitochondrial behavior was recorded only under basal conditions and was not assessed under pathological or pharmacological stress to push protein oxidation mitochondrial membrane potential to extreme levels. Our agent-based model was therefore constructed with these limited data, and therefore caution should be used on interpreting model outputs at outer bounds.

RESOURCE AVAILABILITY

Lead contact

Further information and requests for resources and reagents can be directed to the lead contact, Thomas H. Sanderson (thsand@med.umich.edu).

Materials availability

This study did not generate new unique reagents.

Data and code availability

- Data: original microscopy data reported in this paper will be shared by the lead contact upon request.
- Code: all code for the MiDyS NetLogo model is available on GitHub (https://github.com/sanderson-lab/MiDyS-agent-model). NetLogo is an open-source software that can be run as a web application or downloaded for offline use from: https://www.netlogoweb.org/. Any additional information or data will be made available by the corresponding author by request.
- Additional information: any additional information required to reanalyze the data reported in this paper is available from the lead contact upon request.

ACKNOWLEDGMENTS

We would like to thank Dr. Zhen Yan for the generous gift of conditional MitoTimer mice (Virginia Polytechnic Institute and State University, VA). Figures were constructed using Adobe Illustrator and BioRender. This work was supported through the U.S. National Institutes of Health NINDS grant numbers R01NS120322 (THS) and F31NS124280 (GMF) and NIA grant number F99AG079793 (GMF). Opinions, interpretations, conclusions, and recommendations are those of the authors and are not necessarily endorsed by the National Institutes of Health.

AUTHOR CONTRIBUTIONS

Conceptualization, G.M.F., A.R.A., and T.H.S.; methodology, G.M.F.; investigation, G.M.F., F.J.T.T., and R.L.S.; formal analysis, G.M.F.; supervision, T.H.S.; funding acquisition, G.M.F. and T.H.S.; visualization, G.M.F. and T.H.S.; writing (original draft), G.M.F.; writing (review & editing), G.M.F., A.R.A., and T.H.S.

DECLARATION OF INTERESTS

All authors declare no potential conflict of interest.

STAR★METHODS

Detailed methods are provided in the online version of this paper and include the following:

- KEY RESOURCES TABLE
- EXPERIMENTAL MODEL AND STUDY PARTICIPANT DETAILS
  - Mouse strains
  - Primary neuron culture
- METHOD DETAILS
  - Oxygen-glucose deprivation (OGD)
  - Immunofluorescence and fluorescent microscopy
  - Live-cell microscopy
  - Live-cell image processing/segmentation
  - Automated detection of fission/fusion events
  - Equation fitting/regression
  - MiDyS modeling in NetLogo
  - Fixed mitochondrial morphology analysis
- QUANTIFICATION AND STATISTICAL ANALYSIS

Received: March 27, 2024
Revised: February 24, 2025
Accepted: April 4, 2025
Published: April 8, 2025

REFERENCES

1. Quintana-Cabrera, R., and Scorrano, L. (2023). Determinants and outcomes of mitochondrial dynamics. Mol. Cell *83*, 857–876.
2. Giacomello, M., Pyakurel, A., Glytsou, C., and Scorrano, L. (2020). The cell biology of mitochondrial membrane dynamics. Nat. Rev. Mol. Cell Biol. *21*, 204–224.
3. Archer, S.L. (2013). Mitochondrial dynamics–mitochondrial fission and fusion in human diseases. N. Engl. J. Med. *369*, 2236–2251.
4. Adebayo, M., Singh, S., Singh, A.P., and Dasgupta, S. (2021). Mitochondrial fusion and fission: The fine-tune balance for cellular homeostasis. FASEB J. *35*, e21620.
5. Pernas, L., and Scorrano, L. (2016). Mito-morphosis: mitochondrial fusion, fission, and cristae remodeling as key mediators of cellular function. Annu. Rev. Physiol. *78*, 505–531.
6. Itoh, K., Nakamura, K., Iijima, M., and Sesaki, H. (2013). Mitochondrial dynamics in neurodegeneration. Trends Cell Biol. *23*, 64–71.
7. Anzell, A.R., Maizy, R., Przyklenk, K., and Sanderson, T.H. (2018). Mitochondrial quality control and disease: Insights into ischemia-reperfusion injury. Mol. Neurobiol. *55*, 2547–2564.
8. Fischer, T.D., Hylin, M.J., Zhao, J., Moore, A.N., Waxham, M.N., and Dash, P.K. (2016). Altered mitochondrial dynamics and TBI pathophysiology. Front. Syst. Neurosci. *10*, 29.
9. Robertson, G.L., Riffle, S., Patel, M., Bodnya, C., Marshall, A., Beasley, H. K., Garza-Lopez, E., Shao, J., Vue, Z., Hinton, A., et al. (2023). DRP1 mutations associated with EMPF1 encephalopathy alter mitochondrial membrane potential and metabolic programs. J. Cell Sci. *136*, jcs260370.
10. Cartes-Saavedra, B., Lagos, D., Macuada, J., Arancibia, D., Burté, F., Sjöberg-Herrera, M.K., Andrés, M.E., Horvath, R., Yu-Wai-Man, P., Hajnóczky, G., and Eisner, V. (2023). OPA1 disease-causing mutants have domain-specific effects on mitochondrial ultrastructure and fusion. Proc. Natl. Acad. Sci. USA *120*, e2207471120.
11. Wei, F.L., Wang, T.F., Wang, C.L., Zhang, Z.P., Zhao, J.W., Heng, W., Tang, Z., Du, M.R., Yan, X.D., Li, X.X., et al. (2024). Cytoplasmic escape of mitochondrial DNA mediated by Mfn2 downregulation promotes microglial activation via cGas-Sting axis in spinal cord injury. Adv. Sci. *11*, e2305442.
12. Han, S., Nandy, P., Austria, Q., Siedlak, S.L., Torres, S., Fujioka, H., Wang, W., and Zhu, X. (2020). Mfn2 ablation in the adult mouse hippocampus and cortex causes neuronal death. Cell *9*, 116.
13. Park, S.J., Bae, J.E., Jo, D.S., Kim, J.B., Park, N.Y., Fang, J., Jung, Y.K., Jo, D.G., and Cho, D.H. (2021). Increased O-GlcNAcylation of Drp1 by amyloid-beta promotes mitochondrial fission and dysfunction in neuronal cells. Mol. Brain *14*, 6.
14. Whitley, B.N., Engelhart, E.A., and Hoppins, S. (2019). Mitochondrial dynamics and their potential as a therapeutic target. Mitochondrion *49*, 269–283.
15. Miller, R., Ewy, W., Corrigan, B.W., Ouellet, D., Hermann, D., Kowalski, K. G., Lockwood, P., Koup, J.R., Donevan, S., El-Kattan, A., et al. (2005). How modeling and simulation have enhanced decision making in new drug development. J. Pharmacokinet. Pharmacodyn. *32*, 185–197.
16. Gal, J., Milano, G., Ferrero, J.M., Saâda-Bouzid, E., Viotti, J., Chabaud, S., Gougis, P., Le Tourneau, C., Schiappa, R., Paquet, A., et al. (2018). Optimizing drug development in oncology by clinical trial simulation: Why and how? Briefings Bioinf. *19*, 1203–1217.
17. Luraghi, G., Cahalane, R.M.E., van de Ven, E., Overschie, S.C.M., Gijsen, F.J.H., and Akyildiz, A.C. (2021). In vitro and in silico modeling of endovascular stroke treatments for acute ischemic stroke. J. Biomech. *127*, 110693.
18. Cortassa, S., and Aon, M.A. (2012). Computational modeling of mitochondrial function. Mol. Cell *810*, 311–326.
19. Cortassa, S., Sollott, S.J., and Aon, M.A. (2018). Computational modeling of mitochondrial function from a systems biology perspective. Methods Mol. Biol. *1782*, 249–265.
20. Tewai, S.G., Dash, R.K., Beard, D.A., and Bazil, J.N. (2012). A biophysical model of the mitochondrial ATP-Mg/P(i) carrier. Biophys. J. *103*, 1616–1625.
21. Kleessen, S., Araújo, W.L., Fernie, A.R., and Nikoloski, Z. (2012). Model-based confirmation of alternative substrates of mitochondrial electron transport chain. J. Biol. Chem. *287*, 11122–11131.
22. Senneff, S., and Lowery, M.M. (2022). Computational model of the effect of mitochondrial dysfunction on excitation-contraction coupling in skeletal muscle. Bull. Math. Biol. *84*, 123.
23. Kowald, A., and Klipp, E. (2014). Mathematical models of mitochondrial aging and dynamics. Prog. Mol. Biol. Transl. Sci. *127*, 63–92.
24. Zamponi, N., Zamponi, E., Cannas, S.A., Billoni, O.V., Helguera, P.R., and Chialvo, D.R. (2018). Mitochondrial network complexity emerges from fission/fusion dynamics. Sci. Rep. *8*, 363.
25. Hoffman, T.E., Barnett, K.J., Wallis, L., and Hanneman, W.H. (2017). A multimethod computational simulation approach for investigating mitochondrial dynamics and dysfunction in degenerative aging. Aging Cell *16*, 1244–1255.
26. Sukhorukov, V.M., Dikov, D., Reichert, A.S., and Meyer-Hermann, M. (2012). Emergence of the mitochondrial reticulum from fission and fusion dynamics. PLoS Comput. Biol. *8*, e1002745.
27. Mouli, P.K., Twig, G., and Shirihai, O.S. (2009). Frequency and selectivity of mitochondrial fusion are key to its quality maintenance function. Biophys. J. *96*, 3509–3518.
28. Soheilypour, M., and Mofrad, M.R.K. (2018). Agent-based modeling in molecular systems biology. Bioessays *40*, e1800020.
29. Figge, M.T., Reichert, A.S., Meyer-Hermann, M., and Osiewacz, H.D. (2012). Deceleration of fusion–fission cycles improves mitochondrial quality control during aging. PLoS Comput. Biol. *8*, e1002576.
30. Dalmasso, G., Marin Zapata, P.A., Brady, N.R., and Hamacher-Brady, A. (2017). Agent-based modeling of mitochondria links sub-cellular dynamics to cellular homeostasis and heterogeneity. PLoS One *12*, e0168198.
31. Zorova, L.D., Popkov, V.A., Plotnikov, E.Y., Silachev, D.N., Pevzner, I.B., Jankauskas, S.S., Babenko, V.A., Zorov, S.D., Balakireva, A.V., Juhaszova, M., et al. (2018). Mitochondrial membrane potential. Anal. Biochem. *552*, 50–59.
32. Teodoro, J.S., Palmeira, C.M., and Rolo, A.P. (2018). Mitochondrial membrane potential ($\Delta\Psi$) fluctuations associated with the metabolic states of mitochondria. Methods Mol. Biol. *1782*, 109–119.

33. Xiao, B., Deng, X., Zhou, W., and Tan, E.K. (2016). Flow cytometry-based assessment of mitophagy using MitoTracker. Front. Cell. Neurosci. *10*, 76.

34. Greene, A.W., Grenier, K., Aguileta, M.A., Muise, S., Farazifard, R., Haque, M.E., McBride, H.M., Park, D.S., and Fon, E.A. (2012). Mitochondrial processing peptidase regulates PINK1 processing, import and Parkin recruitment. EMBO Rep. *13*, 378–385.

35. Schindelin, J., Arganda-Carreras, I., Frise, E., Kaynig, V., Longair, M., Pietzsch, T., Preibisch, S., Rueden, C., Saalfeld, S., Schmid, B., et al. (2012). Fiji: an open-source platform for biological-image analysis. Nat. Methods *9*, 676–682.

36. Busch, K.B., Kowald, A., and Spelbrink, J.N. (2014). Quality matters: how does mitochondrial network dynamics and quality control impact on mtDNA integrity? Philos. Trans. R. Soc. Lond. B Biol. Sci. *369*, 20130442.

37. Muster, B., Kohl, W., Wittig, I., Strecker, V., Joos, F., Haase, W., Bereiter-Hahn, J., and Busch, K. (2010). Respiratory chain complexes in dynamic mitochondria display a patchy distribution in life cells. PLoS One *5*, e11910.

38. Ali, S., and McStay, G.P. (2018). Regulation of mitochondrial dynamics by proteolytic processing and protein turnover. Antioxidants *7*, 15.

39. Dewachter, I., Reversé, D., Caluwaerts, N., Ris, L., Kuipéri, C., Van den Haute, C., Spittaels, K., Umans, L., Serneels, L., Thiry, E., et al. (2002). Neuronal deficiency of presenilin 1 inhibits amyloid plaque formation and corrects hippocampal long-term potentiation but not a cognitive defect of amyloid precursor protein [V717I] transgenic mice. J. Neurosci. *22*, 3445–3453.

40. Wilson, R.J., Drake, J.C., Cui, D., Zhang, M., Perry, H.M., Kashatus, J.A., Kusminski, C.M., Scherer, P.E., Kashatus, D.F., Okusa, M.D., and Yan, Z. (2019). Conditional MitoTimer reporter mice for assessment of mitochondrial structure, oxidative stress, and mitophagy. Mitochondrion *44*, 20–26.

41. Hernandez, G., Thornton, C., Stotland, A., Lui, D., Sin, J., Ramil, J., Magee, N., Andres, A., Quarato, G., Carreira, R.S., et al. (2013). MitoTimer: a novel tool for monitoring mitochondrial turnover. Autophagy *9*, 1852–1861.

42. Wilensky, U. (1999). NetLogo (Northwestern University). http://ccl.northwestern.edu/netlogo/.CenterforConnectedLearningandComputer-Based Modeling.

43. Kurz, F.T., Aon, M.A., Schlemmer, H.P., Jende, J.M.E., O'Rourke, B., and Armoundas, A.A. (2023). Fractal dynamics of individual mitochondrial oscillators measure local inter-mitochondrial coupling. Biophys. J. *122*, 1459–1469.

44. Bomba-Warczak, E., Edassery, S.L., Hark, T.J., and Savas, J.N. (2021). Long-lived mitochondrial cristae proteins in mouse heart and brain. J. Cell Biol. *220*, e202005193.

45. Kuznetsov, A.V., Javadov, S., Saks, V., Margreiter, R., and Grimm, M. (2017). Synchronism in mitochondrial ROS flashes, membrane depolarization and calcium sparks in human carcinoma cells. Biochim. Biophys. Acta Bioenerg. *1858*, 418–431.

46. Anzell, A.R., Fogo, G.M., Gurm, Z., Raghunayakula, S., Wider, J.M., Maheras, K.J., Emaus, K.J., Bryson, T.D., Wang, M., Neumar, R.W., et al. (2021). Mitochondrial fission and mitophagy are independent mechanisms regulating ischemia/reperfusion injury in primary neurons. Cell Death Dis. *12*, 475.

47. Jin, S.M., Lazarou, M., Wang, C., Kane, L.A., Narendra, D.P., and Youle, R.J. (2010). Mitochondrial membrane potential regulates PINK1 import and proteolytic destabilization by PARL. J. Cell Biol. *191*, 933–942.

48. Sato, T.K., Kawano, S., and Endo, T. (2019). Role of the membrane potential in mitochondrial protein unfolding and import. Sci. Rep. *9*, 7637.

49. Fogo, G.M., Anzell, A.R., Maheras, K.J., Raghunayakula, S., Wider, J.M., Emaus, K.J., Bryson, T.D., Bukowski, M.J., Neumar, R.W., Przyklenk, K., and Sanderson, T.H. (2021). Machine learning-based classification of mitochondrial morphology in primary neurons and brain. Sci. Rep. *11*, 5133.

50. Chen, S.D., Yang, D.I., Lin, T.K., Shaw, F.Z., Liou, C.W., and Chuang, Y.C. (2011). Roles of oxidative stress, apoptosis, PGC-1α and mitochondrial biogenesis in cerebral ischemia. Int. J. Mol. Sci. *12*, 7199–7215.

51. Iijima, T., Mishima, T., Tohyama, M., Akagawa, K., and Iwao, Y. (2003). Mitochondrial membrane potential and intracellular ATP content after transient experimental ischemia in the cultured hippocampal neuron. Neurochem. Int. *43*, 263–269.

52. Sanderson, T.H., Reynolds, C.A., Kumar, R., Przyklenk, K., and Hüttemann, M. (2013). Molecular mechanisms of ischemia-reperfusion injury in brain: pivotal role of the mitochondrial membrane potential in reactive oxygen species generation. Mol. Neurobiol. *47*, 9–23.

53. Kuzmiak-Glancy, S., Glancy, B., and Kay, M.W. (2022). Ischemic damage to every segment of the oxidative phosphorylation cascade elevates ETC driving force and ROS production in cardiac mitochondria. Am. J. Physiol. Heart Circ. Physiol. *323*, H499–H512.

54. Brookes, P.S., Yoon, Y., Robotham, J.L., Anders, M.W., and Sheu, S.S. (2004). Calcium, ATP, and ROS: a mitochondrial love-hate triangle. Am. J. Physiol. Cell Physiol. *287*, C817–C833.

55. Chatterjee, S., Browning, E.A., Hong, N., DeBolt, K., Sorokina, E.M., Liu, W., Birnbaum, M.J., and Fisher, A.B. (2012). Membrane depolarization is the trigger for PI3K/Akt activation and leads to the generation of ROS. Am. J. Physiol. Heart Circ. Physiol. *302*, H105–H114.

56. Iijima, T., Mishima, T., Akagawa, K., and Iwao, Y. (2006). Neuroprotective effect of propofol on necrosis and apoptosis following oxygen-glucose deprivation–relationship between mitochondrial membrane potential and mode of death. Brain. Res. *1099*, 25–32.

57. Starkov, A.A., and Fiskum, G. (2003). Regulation of brain mitochondrial H2O2 production by membrane potential and NAD(P)H redox state. J. Neurochem. *86*, 1101–1107.

58. Abramov, A.Y., Scorziello, A., and Duchen, M.R. (2007). Three distinct mechanisms generate oxygen free radicals in neurons and contribute to cell death during anoxia and reoxygenation. J. Neurosci. *27*, 1129–1138.

59. Chouchani, E.T., Pell, V.R., Gaude, E., Aksentijević, D., Sundier, S.Y., Robb, E.L., Logan, A., Nadtochiy, S.M., Ord, E.N.J., Smith, A.C., et al. (2014). Ischaemic accumulation of succinate controls reperfusion injury through mitochondrial ROS. Nature *515*, 431–435.

60. Kumar, R., Bukowski, M.J., Wider, J.M., Reynolds, C.A., Calo, L., Lepore, B., Tousignant, R., Jones, M., Przyklenk, K., and Sanderson, T.H. (2016). Mitochondrial dynamics following global cerebral ischemia. Mol. Cell. Neurosci. *76*, 68–75.

61. Wojtyniak, P., Boratynska-Jasinska, A., Serwach, K., Gruszczynska-Biegala, J., Zablocka, B., Jaworski, J., and Kawalec, M. (2022). Mitofusin 2 integrates mitochondrial network remodelling, mitophagy and renewal of respiratory chain proteins in neurons after oxygen and glucose deprivation. Mol. Neurobiol. *59*, 6502–6518.

62. Margaill, I., Plotkine, M., and Lerouet, D. (2005). Antioxidant strategies in the treatment of stroke. Free. Radic. Biol. Med. *39*, 429–443.

63. Ibrahim, A.A., Abdel Mageed, S.S., Safar, M.M., El-Yamany, M.F., and Oraby, M.A. (2023). MitoQ alleviates hippocampal damage after cerebral ischemia: The potential role of SIRT6 in regulating mitochondrial dysfunction and neuroinflammation. Life. Sci. *328*, 121895.

64. Hobbs, C.E., Murphy, M.P., Smith, R.A.J., and Oorschot, D.E. (2008). Neonatal rat hypoxia-ischemia: Effect of the anti-oxidant mitoquinol, and S-PBN. Pediatr. Int. *50*, 481–488.

65. Komakula, S., Bhatia, R., Sahib, A., Upadhyay, A., S, L.J., Garg, A., Y, V.V., Pandit, A.K., Vibha, D., Singh, M.B., et al. (2024). Safety and efficacy of N-acetylcysteine (NAC) as an adjunct to standard treatment in patients with acute ischemic stroke: a randomized controlled pilot trial (NACTLYS). Sci. Rep. *14*, 1103.

66. Mao, R., Zong, N., Hu, Y., Chen, Y., and Xu, Y. (2022). Neuronal death mechanisms and therapeutic strategy in ischemic stroke. Neurosci. Bull. *38*, 1229–1247.

67. Sohrabji, F., Selvamani, A., and Balden, R. (2013). Revisiting the timing hypothesis: biomarkers that define the therapeutic window of estrogen for stroke. Horm. Behav. *63*, 222–230.

68. Waller, J., Kaur, P., Tucker, A., Amer, R., Bae, S., Kogler, A., and Umair, M. (2021). The benefit of intravenous thrombolysis prior to mechanical thrombectomy within the therapeutic window for acute ischemic stroke. Clin. Imaging. *79*, 3–7.

69. Lu, S., Zhang, J., Wu, R., Cao, Y., Xu, X., Li, G., Liu, S., Shi, H., and Wu, F. (2022). Use of machine learning algorithms to predict the outcomes of mechanical thrombectomy in acute ischemic stroke patients with an extended therapeutic time window. J. Comput. Assist. Tomogr. *46*, 775–780.

70. Kleele, T., Rey, T., Winter, J., Zaganelli, S., Mahecic, D., Perreten Lambert, H., Ruberto, F.P., Nemir, M., Wai, T., Pedrazzini, T., and Manley, S. (2021). Distinct fission signatures predict mitochondrial degradation or biogenesis. Nature *593*, 435–439.

71. Chang, X., Niu, S., Shang, M., Li, J., Guo, M., Zhang, W., Sun, Z., Li, Y., Zhang, R., Shen, X., et al. (2023). ROS-Drp1-mediated mitochondria fission contributes to hippocampal HT22 cell apoptosis induced by silver nanoparticles. Redox Biol. *63*, 102739.

72. Cid-Castro, C., and Morán, J. (2021). Differential ROS-mediated phosphorylation of Drp1 in mitochondrial fragmentation induced by distinct cell death conditions in cerebellar granule neurons. Oxid. Med. Cell. Longev. *2021*, 8832863.

73. Iqbal, S., and Hood, D.A. (2014). Oxidative stress-induced mitochondrial fragmentation and movement in skeletal muscle myoblasts. Am. J. Physiol. Cell Physiol. *306*, C1176–C1183.

74. Krzystek, T.J., Banerjee, R., Thurston, L., Huang, J., Swinter, K., Rahman, S.N., Falzone, T.L., and Gunawardena, S. (2021). Differential mitochondrial roles for α-synuclein in DRP1-dependent fission and PINK1/Parkin-mediated oxidation. Cell Death Dis. *12*, 796.

75. Katajisto, P., Döhla, J., Chaffer, C.L., Pentinmikko, N., Marjanovic, N., Iqbal, S., Zoncu, R., Chen, W., Weinberg, R.A., and Sabatini, D.M. (2015). Asymmetric apportioning of aged mitochondria between daughter cells is required for stemness. Science *348*, 340–343.

76. Joshi, D.C., and Bakowska, J.C. (2011). Determination of mitochondrial membrane potential and reactive oxygen species in live rat cortical neurons. J. Vis. Exp. *51*, 2704.

77. Cereghetti, G.M., Costa, V., and Scorrano, L. (2010). Inhibition of Drp1-dependent mitochondrial fragmentation and apoptosis by a polypeptide antagonist of calcineurin. Cell Death Differ. *17*, 1785–1794.

78. De Vos, K.J., Allan, V.J., Grierson, A.J., and Sheetz, M.P. (2005). Mitochondrial function and actin regulate dynamin-related protein 1-dependent mitochondrial fission. Curr. Biol. *15*, 678–683.

79. Twig, G., Elorza, A., Molina, A.J.A., Mohamed, H., Wikstrom, J.D., Walzer, G., Stiles, L., Haigh, S.E., Katz, S., Las, G., et al. (2008). Fission and selective fusion govern mitochondrial segregation and elimination by autophagy. EMBO J. *27*, 433–446.

80. Ferree, A.W., Trudeau, K., Zik, E., Benador, I.Y., Twig, G., Gottlieb, R.A., and Shirihai, O.S. (2013). MitoTimer probe reveals the impact of autophagy, fusion, and motility on subcellular distribution of young and old mitochondrial protein and on relative mitochondrial protein age. Autophagy *9*, 1887–1896.

81. Friedman, J.R., Lackner, L.L., West, M., DiBenedetto, J.R., Nunnari, J., and Voeltz, G.K. (2011). ER tubules mark sites of mitochondrial division. Science *334*, 358–362.

82. Vanden Hoek, T.L., Li, C., Shao, Z., Schumacker, P.T., and Becker, L.B. (1997). Significant levels of oxidants are generated by isolated cardiomyocytes during ischemia prior to reperfusion. J. Mol. Cell. Cardiol. *29*, 2571–2583.

83. Levraut, J., Iwase, H., Shao, Z.-H., Vanden Hoek, T.L., and Schumacker, P.T. (2003). Cell death during ischemia: relationship to mitochondrial depolarization and ROS generation. Clin. Imaging. *284*, H549–H558.

84. Peters, O., Back, T., Lindauer, U., Busch, C., Megow, D., Dreier, J., and Dirnagl, U. (1998). Increased formation of reactive oxygen species after permanent and reversible middle cerebral artery occlusion in the rat. J. Cereb. Blood. Flow. Metab. *18*, 196–205.

85. Nair, S., Leverin, A.L., Rocha-Ferreira, E., Sobotka, K.S., Thornton, C., Mallard, C., and Hagberg, H. (2022). Induction of mitochondrial fragmentation and mitophagy after neonatal hypoxia-ischemia. Cells *11*, 1193.

86. Arganda-Carreras, I., Kaynig, V., Rueden, C., Eliceiri, K.W., Schindelin, J., Cardona, A., and Sebastian Seung, H. (2017). Trainable Weka Segmentation: a machine learning tool for microscopy pixel classification. Bioinformatics *33*, 2424–2426.

87. Legland, D., Arganda-Carreras, I., I., and Andrey, P. (2016). MorphoLibJ: integrated library and plugins for mathematical morphology with ImageJ. Bioinformatics *32*, 3532–3534.

88. Wolf, D.M., Segawa, M., Kondadi, A.K., Anand, R., Bailey, S.T., Reichert, A.S., van der Bliek, A.M., Shackelford, D.B., Liesa, M., and Shirihai, O.S. (2019). Individual cristae within the same mitochondrion display different membrane potentials and are functionally independent. EMBO J. *38*, e101056.

89. Fogo, G.M., Raghunayakula, S., Emaus, K.J., Torres Torres, F.J., Wider, J. M., and Sanderson, T.H. (2024). Mitochondrial membrane potential and oxidative stress interact to regulate Oma1-dependent processing of Opa1and mitochondrial dynamics. FASEB J. *38*, e70066.

STAR★METHODS

KEY RESOURCES TABLE

REAGENT or RESOURCE	SOURCE	IDENTIFIER
Antibodies		
Mouse anti-ATPB	Abcam	ab14730
Goat anti-Mouse Alexa Fluor 488	Invitrogen	A11029
Chemicals, peptides, and recombinant proteins		
APV (2-Amino-5-phosphonopentanoic acid)	Sigma	A-5282
Hibernate-A Medium	Gibco	A1247501
B-27 Supplement	Gibco	17504044
L-cysteine	Sigma	778672
Papain	Worthington	LS 03126
DNase I from bovine pancreas	Roche	11284932001
Neurobasal Plus Medium	Gibco	A3582901
GlutaMax Supplement	Gibco	35050061
Penicillin/Streptomycin Solution	Gibco	SV30010
B-27 Supplement (minus antioxidants)	Gibco	10889038
Goat Serum	Sigma	G9023
MitoTracker Deep Red FM	Fisher Scientific	M22426
Earle's Balanced Salts Solution (no phenol red)	Fisher Scientific	AAJ67559AP
Experimental models: Organisms/strains		
Wild-type (C57BL/6J) mice	The Jackson Laboratory	C57BL/6J
Thy1-Cre (FVB/N-Tg(Thy1-cre)1Vln/J) mice	The Jackson Laboratory	Strain #006143
Conditional MitoTimer mice	Zhen Yan (UVA)[40]	N/A
Software and algorithms		
FIJI	Schindelin et al.[35]	https://imagej.net/software/fiji/
Zeiss Zen Pro	Zeiss	N/A
Morphological Filters Plug-In	Legland et al.[87]	https://imagej.net/plugins/morpholibj
Automated Detection of Fission/Fusion Events .ijm script	This paper	https://github.com/sanderson-lab/MiDyS-agent-model
MiDyS Agent-Based Model	This paper	https://github.com/sanderson-lab/MiDyS-agent-model
RStudio	PBC	N/A
NetLogo	NetLogo	https://ccl.northwestern.edu/netlogo/
GraphPad Prism 9	GraphPad	N/A

EXPERIMENTAL MODEL AND STUDY PARTICIPANT DETAILS

Mouse strains

All procedures were performed in accordance with institutional guidelines and approved by the University of Michigan Institutional Animal Care and Use Committee (IACUC #PRO00011677). Mice were maintained on a 12 h light/dark cycle with standard rodent chow and water available *ad libitum*. Wild-type (WT) mice (C57BL/6J) were purchased from The Jackson Laboratory (Bar Harbor, ME). Thy1-Cre mice[39] were purchased from The Jackson Laboratory (Bar Harbor, ME). Conditional MitoTimer mice were generously provided by Zhen Yan, Virginia Polytechnic Institute and State University, VA.[40]

Primary neuron culture

Cerebral cortices from postnatal day 0–1 (P0–P1) mouse pups (male and female included in mixed cultures) were isolated and minced following sacrifice by decapitation. Tissue was incubated in enzyme digestion solution (Hibernate-A Medium (Gibco, A1247501), 1X B-27 supplement (Gibco, 17504044), 0.06 mg/mL L-cysteine (Sigma, 778672), 1.4 $\times$ 10−2 N NaOH (Sigma, 43617), 10 ng/mL APV (2-Amino-5-phosphonopentanoic acid, Sigma, A-5282), 1:100 Papain (Worthington, LS 03126), 40μg/mL DNase I from bovine

pancreas (Roche, 11284932001) for 30 min at 37°C. Following digestion, tissue was washed with DPBS and dissociated in Hibernate-A medium with 1X B-27. Cell density was measured by hemocytometer and trypan blue staining. For live-cell imaging, cells were seeded onto 0.1% PEI-coated glass coverslips in 6-well dishes (1.5 x 10^6 cells/well). For fixed OGD experiments, cells were plated onto 0.1% PEI-coated glass coverslips in 24-well dishes (0.3 x 10^6 cells/well). After 30 min, complete media change was performed with neurobasal complete medium (1x Neurobasal Plus medium (Gibco, A3582901), 1X B-27 Plus supplement (Gibco, A3653401), 0.5 mM Glutamax Supplement (Gibco, 35050061), and 1% Penicillin/Streptomycin Solution (Gibco, SV30010)). Cells were incubated at 37°C with 5% CO2 for 14 days. Half-media changes were performed every 3–4 days with neurobasal complete medium.

METHOD DETAILS

Oxygen-glucose deprivation (OGD)

Oxygen–glucose deprivation and reoxygenation was performed as previously described.[89] Briefly, EBSS without glucose was bubbled in a hypoxic chamber (Coy Lab Products, maintained at <0.1% O_2, 5% CO_2, and 37°C) with 95% N_2 and 5% CO_2 gas for 60 min for deoxygenation. Neurons were placed inside the chamber and washed 3 times with de-oxygenated EBSS and allowed to incubate for 30 min. Neurons were then removed from the chamber and reoxygenated with Neurobasal Plus medium with 1X B-27 minus antioxidants (Gibco, 10889038) and incubated at 37°C in 5% CO_2. Control condition cells remained at normoxic conditions, were washed 3 times with EBSS with glucose, and changed to Neurobasal Plus medium with 1X B-27 minus antioxidants after 30 min. Neurons were allowed to reoxygenated for either 25 or 60 min. Neurons were either fixed immediately after the 30 min OGD period or after the indicated reoxygenation time with 4% paraformaldehyde (Fisher Scientific, 50980487) for 15 min at 37°C. Samples were then washed 3 times with DPBS and stored at 4°C until immunofluorescent staining.

Immunofluorescence and fluorescent microscopy

Immunofluorescent staining of coverslips was performed as previously described.[89] Briefly, coverslips were incubated in blocking solution (5% goat serum [Sigma, G9023] and 0.3% Triton X-100 [Acros Organics, 215682500] in DPBS) for 60 min at room temperature. Coverslips were then incubated in primary antibody solution (1:1000 mouse anti-ATPB [Abcam, ab14730], 1% BSA [Sigma, A9647], and 0.3% Triton X-100 in DPBS) at 4°C overnight. Coverslips were then washed 3 times in DPBS and incubated in secondary antibody solution (1:200 goat anti-mouse AlexaFluor 488 [Invitrogen, A11029], 1% BSA [Sigma, A9647], and 0.3% Triton X-100 in DPBS for 60 min. Coverslips were mounted on glass slides using Fluoroshield with DAPI (Sigma, F6057) after 3 washes with DPBS.

Live-cell microscopy

On day-in-vitro 14, primary neurons are transferred to a live cell microscopy incubation chamber (37°C with 20.9% O_2 5% CO_2) and allowed to acclimate for 30 minutes. For MitoTracker Deep Red recordings, cells were washed once with sterile PBS and incubated with 30nM MitoTracker Deep Red FM (Fisher Scientific, M22426) in Earle's Balanced Salts Solution (EBSS) without phenol red (Fisher Scientific, AAJ67559AP) during 30 minute acclimation. Neurons were imaged on Zeiss Axio Observer Z1 inverted microscope with LED illumination with 63x objective (0.103um/pixel). Fields of view were focused on neuronal somas and proximal neurites. Z-stacks (0.24μm steps) of MitoTracker Deep Red or MitoTimer signal were acquired every 60 and 120 seconds, respectively. Z-stacks were processed using Zeiss Zen Pro extended depth of focus wavelets method to generate 2D projections. Images were exported in TIFF format for post-processing. LED power, exposure time, and histograms were fixed for all MitoTimer experiments.

Live-cell image processing/segmentation

Image processing and analysis was performed in FIJI.[35] Actions were performed in batches using a custom .ijm script (github). Briefly, mitochondrial signal was processed using the enhance local contrast (CLAHE) algorithm and background signal was subtracted with a rolling ball radius of 10 pixels. For MitoTimer analysis, green and red images were both processed and merged at this step. Mitochondrial objects were segmented using the Trainable Weka segmentation plug-in.[86] Segmented images were then converted to 8-bit binary and segmentation over-estimation was removed using the morphological filters plug-in.[87] Original images (non-processed) and segmented images were then used for downstream analysis.

Automated detection of fission/fusion events

A custom .ijm script was used for the automated detection of mitochondrial fission and fusion events (https://github.com/sanderson-lab/MiDyS-agent-model). Fission events were identified by transposing mitochondrial ROIs from $frame^{n-1}$ onto $frame^{n}$ and counting the number of mitochondrial objects within the original ROI. If more than one object was found in the ROI of the original mitochondrial object, that mitochondria was labeled as a fission object. Fusion events were identified by overlaying mitochondrial ROIs from $frame^{n}$ onto $frame^{n-1}$ and counting the number of mitochondrial objects in that ROI. If more than one object was found in the ROI of the resultant mitochondrial object, those objects were labeled as fusion objects. Fusion and fission labeled object ROIs were stored and fusion and fission events were quantified as the number of fission/fusion events divided by the total number of mitochondrial objects in a frame. For the quantification of intrinsic variables of mitochondrial objects, size/shape parameters were measured from segmented images and fluorescence intensity (MitoTracker Deep Red or MitoTimer green and red) were measured from ROIs

overlays onto original (un-processed) channel images. Measurements were taken from all mitochondrial objects, fission-labeled objects, and fusion-labeled objects. Stable objects were then identified by removing fission and fusion-labeled objects from the list of all mitochondrial objects. Mitochondrial measurements were saved as .csv files for further analysis in GraphPad Prism.

Equation fitting/regression

All data analysis, equation fitting, and quantification was performed in GraphPad Prism 9. Frequency distributions of stable, fusion, and fission mitochondrial objects were generated of intrinsic variables from MTDR and MitoTimer recordings. Many biological variables have floor effects that limit measures from falling below zero. These parameters were $\log_{10}$ transformed to allow for easier visualization and modeling of distribution. Gaussian curves were fit to frequency distributions for visual reference and analysis of normality. MitoTimer ratio data presented as non-normal and sums of two gaussian curves were generated for reference.

Classification and predictive modeling of mitochondrial objects was performed using variables that could easily be translated to and quantified in the agent-based modeling software NetLogo. For both MitoTimer and MitoTracker Deep Red data, multiple logistic regression was performed between fission and stable objects, and fusion and stable objects for the generation of four total regression models. Regression models were generated with intercept value, major axis, minor axis, log(area), log(aspect ratio), and log(MTDR or MitoTimer ratio). ROC curves and predicted probability violin plots were created to assess model performance.

MiDyS modeling in NetLogo

Modeling of mitochondrial dynamics was performed using NetLogo, an open source software for the creation and utilization of agent-based models.[42] A 50x50 patch simulation environment was set up in NetLogo with each patch representing a 1x1μm area. Our NetLogo model, called MiDyS, was coded for two procedure sequences: setup and main (go). Our NetLogo model can be accessed via GitHub (https://github.com/sanderson-lab/MiDyS-agent-model).

During setup, individual agents (default termed turtles in NetLogo) represent discrete mitochondrial units with an individual size of 0.5μm. Agents are randomly distributed at setup with a sum determined by the user on the interface panel. At creation, agents are assigned intrinsic variables (“turtles-own”) including age, membrane potential, and mitotimer ratio. Membrane potential and mitotimer ratios were assigned during setup using a normal random distribution, matching the gaussian distribution equations fit to log(MTDR) and log(MitoTimer ratio) distributions from live cell recordings. Initial Networking Density, a user-defined variable, then determines the extent of mitochondrial fusion during setup. Agents run a probability test based on the initial networking density to determine if they will fuse with neighboring agents. If an agent fuses with another agent, a link is created between those two agents. After initial networking, objects are then numbered to encode connected mitochondrial objects. A mitochondrial object is the sum of all agents connected in a network of links. These objects model the fused network morphology of mitochondria in a basal state.

At the conclusion of setup and during the go procedure, each individual agent performs calculations to determine derived intrinsic variables and fission/fusion probabilities. Each agent in the simulation calculates area, major axis, minor axis, aspect ratio (AR), and two fusion and fission probabilities. Equations for area in MiDyS is below in units of μm:

$$area = (0.5 * (sum\ of\ agents\ in\ object)) + (0.3 * (sum\ of\ link\ lengths\ in\ object)$$

Major and minor are defined as the farthest and shortest distances in μm between agents within a mitochondrial object. AR is the major/minor ratio. Because individual agents are connected into mitochondrial objects, all agents within an object share size and shape measurements. However, individual agents hold distinct membrane potential and MitoTimer values even when connected in an object. This behavior intends to model the local differences and compartmentalization often observed across large mitochondrial objects *in vitro*.[88] The variables area, major, minor, aspect ratio, membrane potential ($\Delta\Psi$) and MitoTimer ratio are utilized to calculate the probability that a mitochondrial agent will perform fission and/or fusion. Probabilistic equations were determined by multiple logistic regression of these variables from *in vitro* mitochondrial recordings. The framework for probabilistic equations for fission/fusion (p_f) are listed below:

$$p_f = \frac{e^{(b_0+(b_1)(log(area))+(b_2)(major)+(b_3)(minor)+(b_4)(AR)+(b_5)(\Delta\Psi))}}{1+e^{(b_0+(b_1)(log(area))+(b_2)(major)+(b_3)(minor)+(b_4)(AR)+(b_5)(\Delta\Psi))}}$$

$$p_f = \frac{e^{(b_0+(b_1)(log(area))+(b_2)(major)+(b_3)(minor)+(b_4)(AR)+(b_5)(mitotimer))}}{1+e^{(b_0+(b_1)(log(area))+(b_2)(major)+(b_3)(minor)+(b_4)(AR)+(b_5)(mitotimer))}}$$

No *in vitro* data was obtained that included simultaneous recordings of mitochondrial membrane potential and MitoTimer ratio, therefore two separate equations were generated and encoded in the agent-based model. Agents choose the higher resulting probability between the two equations to define their true fusion or fission probability.

During the go procedure, each agent may move or migrate within the simulation environment. Headings are randomized and each agent has a 50% probability of moving 0.5μm. Movement is restricted if link length reaches the maximum allowed value. If an agent has one or more links to other agents, a fission probability check is performed. If a random value 0-100 falls below the calculated fission probability for a given agent, that agent breaks the link with its link neighbor that has the highest fission probability. If an agent has an unlinked neighbor within 2.5μm of itself, a fusion check is performed. If a random value 0-100 falls below the fusion probability for a given agent, that agent will create a new link to the local agent with the highest fusion probability. Mitochondrial objects are

re-numbered and measured after both fission and fusion procedures. Agents may be removed from the simulation via the mitophagy function. Unlinked agents have an equal 10% chance of being removed by mitophagy after fission and fusion procedures. Surviving agents then have intrinsic age, membrane potential, and MitoTimer adjusted. Age is increased by one after each tick of time. Mitochondrial membrane potential is encoded as the log transformation of relative MTDR intensity and fluctuates by random iterations between ± 0.07 arbitrary units. MitoTimer drifts negative as a function of the absolute value of membrane potential:

$$Mitotimer = (r_{-0.05-0}) * abs(\Delta\Psi)$$

In which, $r_{-0.05-0}$ is a random value between (-0.05) and 0. This equation intends to model the oxidation of MitoTimer over time and the dependence of that oxidation on physiological membrane potential. Membrane potential is encoded in MiDyS as a log transformation of the relative intensity of MTDR signal. Therefore, the further membrane potential deviates from zero, the further it leaves the basal range of membrane potential. The emergence of new agents is dependent on the biogenesis function. Biogenesis occurs at a rate of 5% for all agents in the simulation. Agents undergoing biogenesis (parents) create and link with a newborn agent. The newborn agent is assigned an age of zero, membrane potential according to normal distribution described above, and the MitoTimer value of the parent + 0.14. In order to perform biogenesis, a parent agent must have a membrane potential between (-0.2) and 0.2, and have open space on neighboring patches.

At the conclusion of migration, fission, fusion, mitophagy, aging, and biogenesis, the main procedure is complete. The user interface panel window and variable plots are updated, along with a global descriptor of network dynamics. This global variable, termed the fission/fusion index (FFI), ranges from -1 (fully fragmented) to 1 (highly fused) and is calculated as follows:

$$FFI = 2 * \frac{\#\ of\ agents\ with\ >1\ link}{\#\ of\ total\ agents} - 1$$

Manipulations to membrane potential and MitoTimer oxidation can be tuned on the MiDyS user interface. These variables alter membrane potential and MitoTimer by a percentage of a set increment. Changes in these intrinsic parameters can be visualized via the window (with view-options) and on plots to the right.

Fixed mitochondrial morphology analysis

Immuno-stained neurons were imaged on confocal Zeiss LSM 980 with 63x oil immersion objective (0.132 μm/pixel) at 7 frames per Z-stack (0.24 μm steps). Z-stacks were processed using Zeiss Zen Pro extended depth of focus (wavelets method) and exported as TIFFs for further processing.

Immunofluorescent images of fixed neuronal mitochondria were analyzed using a semi-automated morphological classification pipeline.[49] Compressed z-stack TIFFs of mitochondrial signal (ATPB) were imported into FIJI.[35] Images were converted to 8-bit, contrast was enhanced using Contrast Limited Adaptive Histogram Equalization (CLAHE), and background was subtracted with a rolling ball radius of 10 pixels. Discrete mitochondrial objects were segmented using a Trainable Weka Segmentation plug-in.[86] Segmented images were converted to binary, and 32 size/shape measurements were taken from each mitochondrial object. Measurements were input into a trained randomforest algorithm in RStudio (RStudio, PBC, Boston, MA) for classification to one of four morphologies: network, unbranched, punctate, or swollen. Each individual object was classified, and the percent mitochondrial area for each morphology was calculated per biological replicate. Fusion/fission index was quantified as described above, with mitochondrial area in the network and unbranched morphology in the numerator and total mitochondrial area in the denominator.

QUANTIFICATION AND STATISTICAL ANALYSIS

Quantitative and statistical analyses were performed in Prism 9 (GraphPad Software, Boston, MA). Non-linear curves were fitted using the indicated equations. Final output data from antioxidant simulations was compared using One-Way ANOVA with multiple comparisons against the I/R condition, corrected using Dunnett's method. $p < .05$ was considered statistically significant and is indicated by *.